Automated Diffuser Shape Optimization based on CFD Simulations and Surrogate Modeling

M. Dehghani[1], H. Ajam[2†] and S. Farahat[1]

[1] *Department of Mechanical Engineering, University of Sistan and Baluchestan, Zahedan, 98135-161, Iran*
[2] *Department of Mechanical Engineering, Ferdowsi University of Mashhad, Mashhad, 91775-1111, Iran*

†*Corresponding Author Email: h.ajam@um.ac.ir*

ABSTRACT

An approach for the optimization of laminar flow in diffusers is presented. The goal in our optimization process is to maximize diffuser performance and, in this way, pressure recovery by optimizing the geometry. Our methodology is the optimization through wall contouring of a given two-dimensional diffuser length ratio. The developed algorithm uses the CFD software: Fluent for the hydrodynamic analysis and employs surrogate modeling and an expected improvement approach to optimization. The non-uniform rational basic splines (NURBS) are used to represent the shape of diffuser wall with three to nine design variables, respectively. The framework is assisted by the construction of Kriging model, for the management of the problem. The CFD software and the Kriging model have been combined for a fully automated operation using some special control commands on the MATLAB platform. In order to seek a balance between local and global search, an adaptive sample criterion is employed. The optimal design exhibits a reasonable performance improvement compared with the reference design.

1. INTRODUCTION

Diffusers are the integral parts of many flow systems. An improperly designed diffuser may lead to flow separation and excessive consumption of pumping power. It may also produce a flow mal-distribution in the downstream, which is not acceptable in many applications. Moreover, a constraint of restricted length is often imposed on the design. As a result, designing the optimum shape of a diffuser had been the subject of investigation for many researchers during the last decade. The profile of a plane diffuser with given upstream width and length had been optimized to obtain the maximum static pressure rise by (Cabuk and Modi 1992). The steady-state Navier–Stokes equation was used to model the flow through the diffuser considering two dimensional, incompressible and laminar flow. A set of adjoint equations had been solved to get the direction and relative magnitude of change in the diffuser profile that leads to a higher pressure rise. Geometries for three-dimensional viscous flow had been optimized by (Svenningsen *et al*. 1996), applying quasi-analytical sensitivity analysis. The optimization tool had been applied on a two-dimensional laminar diffuser in order to maximize the pressure recovery by contouring the divergent wall section

and the performance of the diffuser was found to improve by about 5% compared with that of straight-walled geometry. (Cholaseuk *et al*. 1999) explored the optimum design of fluid flow devices using designed numerical experiments, and the stability (robustness) of such designs, respectively. The search pattern during the optimization process was suggested by the design of experiment methodology. The proposed framework was tested with one potential flow problem and two laminar-flow diffuser problems.

In recent years, optimization based on flow analysis is becoming increasingly popular in the field of engineering design. In some cases, evolutionary algorithms are used to ensure reaching the global optimum. Genetic Algorithm (GA) and commercial software Fluent had been used to optimize the shape of a two-dimensional diffuser subjected to incompressible turbulent flow by (Ghosh *et al*. 2009). In their shape optimization problem the values of area ratio and length ratio were kept fixed. (Mariotti *et al*. 2013) developed a passive control of laminar boundary layer separation in a two-dimensional symmetrical diffuser using GA and commercial software Fluent. Their control method was consisted of modifying the geometry of the diffuser walls using contoured cavities with suitable shape.

However, the high computational costs associated with evaluating a large number of objective functions prevent applications of evolutionary algorithms to practical engineering design problems. In order to cut the prohibitive costs, a low fidelity surrogate model can be used to reduce the number of required objective function evaluations. (Queipo *et al.* 2005) and (Simpson *et al.* 2001) reviewed various surrogate models used in engineering design. (Madsen *et al.* 2000) demonstrated the utility of response surface model in a diffuser design. (Marjavaara *et al.* 2007) optimized the shape of a simplified hydraulic turbine diffuser using response surface and radial basis neural network based optimization strategy in conjunction with an evolutionary algorithm. A diffuser had been optimized using the support vector mechanics (SVM) by (Fan *et al.* 2005).The SVM was used to construct a response surface. In that study, the optimization was performed on an easily computable surrogate space. Efficient global optimization method had been used to S-duct diffuser shape design by (HyoGil Bae *et al.* 2012). They controlled the radius of the S-duct by the Hicks–Henne bump function with two design variables.

In the present work, a fully automated aerodynamic optimization system has been developed on the MATLAB platform. The system has four components: the geometry parameterization modeling module, the structured mesh generator Gambit, the aerodynamic simulator Fluent, and the Kriging surrogate based optimizer. The shape optimization for a two-dimensional symmetric diffuser is numerically performed to maximize the area averaged pressure recovery coefficient while subjecting to geometrical constraints. Results show that the aerodynamic performance of the diffuser model can be improved. Also, the effect of area ratio variation along with the shape of diffuser is considered simultaneously. Finally, a comprehensive investigation has also been done to explore the details of optimization process for the case of best performance.

2.   PROBLEM STATEMENT

The considered diffuser geometry is plane symmetric diffuser used by (Cholaseuk *et al.* 1999). Since it is not "a priori" obvious that a symmetric diffuser has a symmetric flow inside, a preliminary validation of the set-up for the simulation of the reference (or original) half-diffuser with the simulation of the whole diffuser is done. The results show that two recirculation regions occur in the whole diffuser: the flow separates at the beginning of the diffuser diverging walls on both sides, the sizes of the two recirculation regions are nearly identical and the flow remains symmetric inside the whole diffuser. The aim of the present problem is to determine the optimum shape of the diffuser in such a way that increase the pressure recovery and decrease pressure loss.

Due to symmetry, only the symmetric half of the diffuser is considered and is shown in Fig. 1. The

geometry constraints are: prescribed inlet width H, prescribed diffuser length 3H, constant length inlet and outlet sections of size 0.75H and 6H respectively. It is important to mention that such a long length after the diffuser has been considered to ensure a proper development of the flow. Note that in all the figures dimensionless coordinates are used, i.e. X=x/H and Y=y/H (capital letters are used for dimensionless parameters and lowercase letters for dimensional quantities). In order to increase the flexibility of optimization the diffuser area ratio is not fixed (1.8≤AR≤ 2.8).

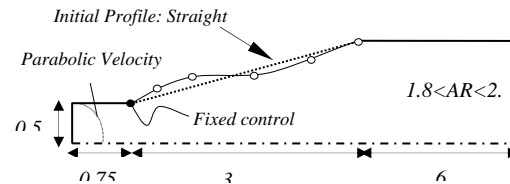**Fig. 1. Plane symmetric diffuser.**

The incompressible flow with a density of 1.225 kg/m^3 and a viscosity of 1.7894*10^-5 kg/m.s enters the domain with a parabolic velocity profile corresponding to a fully developed laminar channel flow. The flow through the diffuser is assumed laminar with the Reynolds number of Re = 100, Re=u_iH/ν where ν is the kinematic viscosity of the fluid and u_i is the average inlet velocity. The diffuser centerline has symmetry boundary conditions and the upper wall is a no-slip wall. The zero diffusion flux condition applied at outlet cells (i.e. the conditions of the outlet plane are extrapolated from within the domain and have no impact on the upstream flow). This kind of boundary condition is approached physically in fully-developed flows. Solving the fluid flow problem, one can find out the velocity and pressure fields from the inlet to the outlet. The pressure rise depends upon the flow rate through the diffuser, characterized by the Reynolds number. A nondimensional pressure rise is defined by a pressure coefficient C_P given as,

$$C_P = (P_o - P_i) / (\tfrac{1}{2}\rho u_i^2) \qquad (1)$$

Where P_0 and P_i are the area averaged diffuser outlet and inlet pressures and ρ is the fluid density.

3.   METHODOLOGY

The main components of the adopted methodology of optimization are geometry parameterization, computational mesh generator *and* CFD solver (i.e. exact solver), surrogate modeling, adaptive optimization based on the above components (geometry parameterization, exact solver and created surrogate model) and to devise a computational algorithm that will combine the outlined components in a monolithic platform for a fully automated operation.

3.1 Geometry Parameterization

As shown in Fig. 1, non-uniform rational basic spline (NURBS) is used to represent the diffuser wall. Though an edge with a varying curvature can be defined by various different curves such as spline, Bezier; NURBS offers a number of flexibilities. As the NURBS uses a parametric functional relationship for the given control points, it does not face any difficulty in treating slopes of extreme values. Any geometrical complexity can be adequately captured, as the curve is represented by a number of low degree polynomials using a unique definition for the entire length. A NURBS curve of degree n is a piecewise rational polynomial function, wherein the numerator and denominator are non-periodic B-splines of degree n.

The first control point of each NURBS curve is located exactly at the inlet, and the other changeable control points are considered design variables. The x-coordinate of the last control point kept fixed during the optimization process, and the other changeable control points are free to shift in x and y directions. The control points were successively increased beginning with 3 points up to a maximum of 6 control points. Since the first control point is fixed at the inlet and the last control point can move only in y-direction, the numbers of design variables are 3, 5, 7 and 9 for three to six control points, respectively.

The coordinates of each control point are constrained by the upper and lower bounds. These upper and lower bounds vary with the number of control points or design variables used to construct the wall shape. Since the x-coordinates of the first and last control points are kept fixed, the general form of the constraints for x coordinate of internal control points is given below for all the four cases

$$\left[(m-1)(\frac{L}{n_{cp}-2}) \le x_m \le m(\frac{L}{n_{cp}-2}) \right]$$ (2)

$$3 \le n_{cp} \le 6, \qquad 1 \le m \le n_{cp} - 2$$

Where m is integer, x_m denotes the x coordinate of the mth internal control point and n_{CP} stand for the total number of control points. Since the area ratio is selected as a design variable, the upper and lower bounds of y coordinates for all n_{CP} control points (except the first control point) have been kept the same, as expressed below

$$0.5H \le y_m \le AR \times 0.5H$$ (3)

3.2 Computational Mesh Generator *and* CFD Solver

The best design of diffuser should have a maximum C_P. To find out C_P, one needs to solve the mass and momentum conservation equations along with appropriate boundary conditions for a given geometry of the diffuser. The commercial CFD software, Fluent, has been used for this purpose. It discretizes the conservation equations by a finite volume technique and solves them. The mesh for the discretization has been created by the software called Gambit. A second-order upwind discretization scheme was used for the momentum equations. SIMPLE algorithm was used for pressure-velocity coupling. The discretized equations are solved implicitly in sequence, starting with the pressure equation followed by the momentum equations and finally by the pressure correction equation. The convergence criterion consisted of monitoring pressure recovery values and reduction of scaled residuals to 10^{-6}. Adequate sensitivity analyses have been carried out to reach the independence of the results from the grid resolution. As shown in Table 1, three different grid resolutions have been considered in the x − y plane. Grid independence was checked on the pressure recovery coefficient, defined in Eq. (1).

Table 1 the mesh convergence details

Grid nodes	C_P
55×10	0.416
110×20	0.428
165×30	0.431

The results obtained on the two finest grids showed a difference of less than 0.1%. Therefore, the 2D grid having 110 × 20 nodes was chosen for the analysis. In order to validate the result of Fluent solver with the CAFFA flow code used by (Cholaseuk *et al*. 1999) the C_P values are compared for a typical straight wall diffuser with fixed area ratio. Although the Fluent predicts a C_P value that is 4.4% higher but is within the accepted range and verify the accuracy of current flow solver.

3.3 Surrogate Modeling

There are a multitude of popular techniques for constructing surrogates in the literature (see e.g. (Jones 2001), (Jin 2005), (Keane and Nair 2005) and (Forrester *et al*. 2008)). Techniques such as Kriging or support vector machines are more ideally suited to global optimization studies since they offer greater flexibility in tuning model parameters and provide a confidence interval of the predicted output. Neural networks require extensive training and validation yet have also been a popular technique for design applications notably in aerodynamic modeling.

There are many different types of Kriging. Ordinary Kriging is a special case of universal Kriging, which is the most widely used method for approximating computational models. It can be written as a combination of a regression model and a random process.

$$1 - C_p(x) \equiv y(x) = \mu + z(x)$$ (4)

Where x is a n_{dv} (number of design variables) dimensional vector, y(x) (i.e. objective function) the unknown function of x, μ an unknown constant trend and z(x) the realization of a stationary normal distributed Gauss random process with zero mean, variance and non-zero covariance. The covariance matrix of z(x) is given by Eq. (5).

$$Cov\,[z\,(x^{\,i}\,),z\,(x^{\,j}\,)] = \sigma^2 \Re[R\,(x^{\,i}\,,x^{\,j}\,)], i\,, j = 1,...,n_s \tag{5}$$

Where $\Re$ is a $n_s \times n_s$ symmetric correlation matrix with values of unity along the diagonal, and R (x^i, x^j) is the spatial correlation function between any two points x^i and x^j of n_s observed points. Variograms, as the cornerstone in Kriging system, are introduced to describe the variance of the difference between two observed points. Since variograms are negative definite, numerically they are harder to handle. Compared with the variogram, a correlogram is easier to work with since all correlograms are positive definite. We adopt the Kriging model based on the correlogram rather than the usual variogram. A popular correlogram is the Gauss spatial correlation function, which is defined as the following form

$$R\,(x^{\,i}\,,x^{\,j}\,) = \exp(-\sum_{k=1}^{n_{dv}} \theta_k \left\| x_k^{\,i} - x_k^{\,j} \right\|^2) \tag{6}$$

Where θ_k is the kth element of correlation vector θ. The Kriging predictor is

$$\hat{y}\,(x) = \hat{\mu} + r(x)^T \Re^{-1}(Y - F\hat{\mu}) \tag{7}$$

Where F is a column vector of length n_s filled with ones, Y the column vector with responses of observed points, and r(x) the correlation vector,

$$r(x) = [R\,(x\,,x^{\,1}),R\,(x\,,x^{\,2}),...,R\,(x\,,x^{\,n_s}\,)]^T \tag{8}$$

For a given θ, $\hat{\mu}$ and $\hat{\sigma}^2$ can be defined as

$$\hat{\mu} = (F^T \Re^{-1} F)^{-1} F^T \Re^{-1} Y \tag{9}$$

$$\hat{\sigma}^2 = (Y - F\hat{\mu})^T \Re^{-1}(Y - F\hat{\mu})/n_s \tag{10}$$

The mean squared error at *x* is given by Eq. (11), indicating the uncertainty of the estimated value

$$s^2(x) = \hat{\sigma}^2 (1 - r^T \Re^{-1} r + (1 - F\Re^{-1}r)^2/(F^T \Re^{-1} F)) \tag{11}$$

Note that $\hat{\mu}$, $\hat{\sigma}^2$, r and $\Re$ implicitly depend on the unknown correlation vector θ. Correlation vector θ of the best Kriging model can be obtained by maximizing the following likelihood function,

$$\ln(\theta) = -\hat{\sigma}^2 \det(\Re)^{\frac{1}{n_s}} \tag{12}$$

Kriging calculations require inversion of the covariance matrix. As observed points begin to cluster around the optimum, the covariance matrix becomes ill-conditioned. It will result in significant numerical inaccuracies when computing the matrix inversion. In order to ensure the most reliable accuracy of the Kriging surrogate, a special numerical technique is adopted (Booker *et al.* 1999).

Once the Kriging surrogate is constructed, the optimum point can be searched over the model. However, this can easily lead to the optimization process falling into a local optimum, because the

surrogate model includes uncertainty at the predicted point. For a robust search of the global optimum in the surrogate model, an expected improvement function (Jones 2001) is used in this application. The function involves computing the possible improvement at a given point *x*. It is assumed that y(x) at *x* is normally distributed with mean $\hat{y}(x)$ and variance $s^2(x)$. For a minimization problem, let y_{min} be the current best objective function value, then an improvement can easily be computed by the following formula:

$$I(x) = \begin{cases} y_{min} - y(x) & y(x) < y_{min} \\ 0 & otherwise \end{cases} \tag{13}$$

The likelihood of this improvement is given by normal density function

$$(1/\sqrt{2\pi}\,s(x))\exp[-(y_{min} - I - \hat{y}(x))^2/(2s^2(x))] \tag{14}$$

Then the expected value of the improvement can be found by integrating over this density function

$$E[I(x)] = \int_0^\infty I \begin{cases} (1/\sqrt{2\pi}\,s(x)) \\ \exp[-(y_{min} - I - \hat{y}(x))^2/(2s^2(x))] \end{cases} dI \tag{15}$$

By integrating by parts, Eq. (15) can be written as,

$$E[I(x)] = s(x)[u\Phi(u) + \Psi(u)] \tag{16}$$

Where Φ and Ψ denote the cumulative distribution function and the probability density function of the standard normal distribution, respectively, and

$$u = (y_{min} - \hat{y}(x))/s(x) \tag{17}$$

The first term on the right side of Eq. (16) is the difference between the current minimum y_{min} and the predicted value $\hat{y}(x)$ at *x*, multiplied by the probability that $\hat{y}(x)$ is smaller than y_{min}. Hence the first term is large when $\hat{y}(x)$ is likely to be smaller than y_{min}. The second term on the right side of Eq. (16) is a product of root mean squared error s(x) and normal density function $\Psi(u)$. It is large when the predicted value $\hat{y}(x)$ is close to y_{min} and s(x) is large. Therefore, the expected improvement function will tend to be large at a point with the predicted value smaller than y_{min} and/or with high predicted uncertainty. Eq. (16) provides an intelligent automatic balance between local exploitation and global exploration. Based on the above statements, the point where the value of the expected improvement function is maximized is used to update the Kriging model.

4.3 Adaptive Optimization Algorithm

For clarification, the overall optimization procedure is organized as the following steps:

1. Define the optimization problem. This includes determination of objective function and parameterization based on design variables and constraint conditions. The objective function in this study is (1-C_P).

2. Generate initial sample points by Design of Experiment technique. In this paper, Space-Filling Latin Hypercube Sampling (SFLHS) based on the maximin metric (Johnson *et al*. 1990), 'tie-breaker' definition and scalar-valued criterion function (Morris and Mitchell 1995) defined to rank competing sampling plans is used.

3. Calculate responses at initial sample points using high fidelity solver. The commercial CFD simulator Fluent is used to solve the Navier-Stokes equations based on the assumption of steady incompressible flow.

4. Construct Kriging surrogate model based on the sample points and corresponding responses.

5. Maximize the expected improvement function to get an additional sample point, and calculate its response using high fidelity solver.

6. Check loop termination. If the convergence criterion is satisfied or computational budget is finished, then stop; otherwise add the additional sample point into the sample points set, and go to step 4. Here, the maximum computational budget is limited to $20n_{dv}$ iterations.

According to (Huang *et al*. 2006) the convergence criterion is chosen as

$$(E[I(x)]_{max} / |y_{max} - y_{min}|) < \varepsilon \tag{18}$$

An advantage of this convergence criterion is that the user can set the convergence tolerance ε without considering the magnitudes of responses for different optimization problems.

In this paper, genetic algorithm (GA) is adopted to maximize the log-likelihood and the expected improvement function.

Finally, an algorithm has been designed, such that the outlined steps combine with each other seamlessly and data transfer takes places without any manual intervention. In this task, the main challenge lies in embedding highly structured commercial softwares like Fluent and Gambit inside an indigenously developed control loop. This has been achieved through an algorithm coded on the Matlab platform. The algorithm is schematically shown in Fig. 2.

At the time of launching, Gambit and Fluent start with their respective journal files. Gambit journal file contains all the required instructions to create mesh file in their proper sequence and similarly, the Fluent journal file contains the instructions needed to solve the velocity and the pressure fields.

4. RESULTS AND DISCUSSION

As outlined above and depicted in Fig. 2, the optimization procedure will start with selection of design variables or control points ($3 \le n_{CP} \le 6$). To generate initial sampling plan, Space-Filling Latin Hypercube Sampling (SFLHS) with $10n_{dv}$ sample is created. After geometry parameterization, mesh generation and CFD simulation the Kriging

surrogate model is created and expected improvement is maximized. In order to maximize the log-likelihood and expected improvement a GA with population size of 20, mutation rate of 0.25, rank weighting approach and single point crossover is used. By determination of next infill vector of variables the geometry parameterization, mesh generation and CFD simulation is done. Finally, the Kriging surrogate model is reconstructed and the optimization is repeated until loop termination.
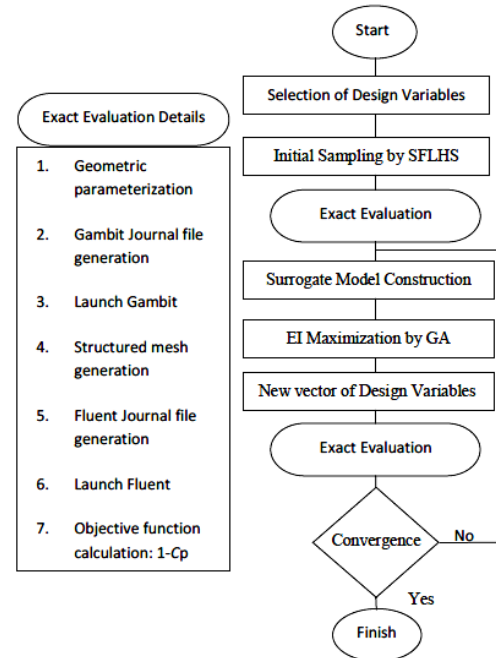

Fig. 2. Schematic of the overall optimization procedure.

Before running the optimization algorithm, in order to find the best straight wall diffuser a set of preliminary runs are performed and a plot of C_P versus AR for all the direct solutions are shown in Fig. 3. With respect to Fig.3 the straight wall diffuser with AR=2.3 is selected as the reference diffuser.
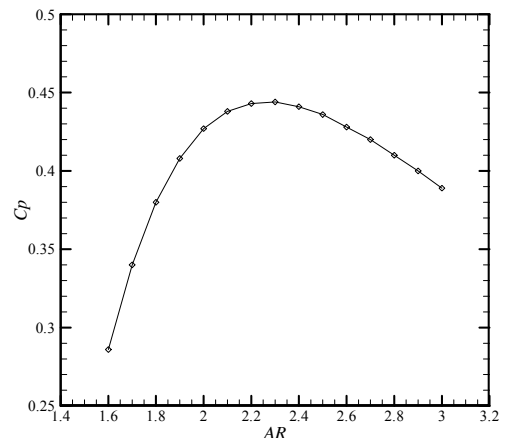

Fig. 3. Pressure recovery coefficient vs. area ratio for straight wall diffusers with *L/H*=3, Re=100.

The streamline pattern obtained for the best straight wall (reference) diffuser is shown in Fig. 4. The C_P value has been obtained as 0.444 for this case.
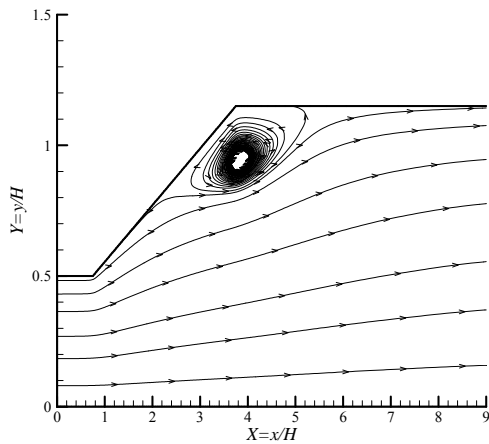

Fig. 4. Streamline pattern in the reference diffuser with straight wall.

This section presents an overall performance comparison between the reference and the optimal designs. In addition, the corresponding flow fields as characterized by pressure recovery coefficients and streamlines are also compared in order to comprehend the flow behavior resulting from the shape optimization. Also, in the previous studies the area ratio of the diffuser was kept fixed and some correlations were developed for the relationship between the area ratio and the optimized diffuser dimensions. Here, the diffuser area ratio is selected as a continuous design variable (1.8≤AR≤2.8). So, the current study offers some important insights into the effect of area ratio on the performance of diffuser.

The optimum diffuser designs as obtained by selecting a number of control points along the diffuser wall (Fig. 1) are described briefly. As mentioned earlier, the number of control points has also been varied to explore various design options. The coordinate values have been obtained as the function of inlet width (H) to generalize the optimum solution. Table 2 shows the C_P values obtained with different number of control points and their optimal positions.

It is interesting to note that an increase in the number of control points does not increase C_P monotonically. In accordance with the results of (Ghosh *et al*. 2009) for a similar turbulent flow optimization, the magnitude of C_P starts falling as the numbers of control points exceed five. Furthermore, In accordance with the results of (Cholaseuk *et al*., 1999) the optimum diffuser profile has a lower area ratio than the best straight walled diffuser and yet produced a larger pressure rise.

At this point, the performance of the optimum diffuser may be compared with that of reference diffuser (Fig.4) to assess the benefit of the optimum

design. It may be recalled that the value of C_P for the reference diffuser has been obtained as 0.444. Compared with that, any design shown in Table 2 shows a rational improvement. To have a better appraisal for the various optimum designs presented in Table 2, streamline pattern for the four different cases is shown in Fig. 5.

Table 2 Values of C_P with different number of control points and their optimal positions

n_{cp}	n_{dv}	C_P	No.	X cord	Y cord	AR
3	3	0.47066	1st 2nd 3rd	0.75H 1.2H 3.75H	0.5H 0.67H 0.96H	1.92
4	5	0.47462	1st 2nd 3rd 4th	0.75H 1.35H 2.52H 3.75H	0.5H 0.74H 0.87H 1.01H	2.02
5	7	0.47619	1st 2nd 3rd 4th 5th	0.75H 1.09H 2.57H 2.94H 3.75H	0.5H 0.65H 0.87H 0.92H H	2
6	9	0.47538	1st 2nd 3rd 4th 5th 6th	0.75H 1.26H 1.9H 2.35H 3.65H 3.75H	0.5H 0.71H 0.81H 0.86H 0.97H 0.98H	1.96

Also, the predicted separation and reattachment positions for various design options are compared in Table 3.

In all the four cases, one can observe the reduction of the separation extent. In addition, two cases show the existence of secondary separation without any notable recirculation region. At last, it is evident that in the best diffuser design flow separates at the initial part of diffuser but reattaches immediately downstream, forming a recirculation region; furthermore, the subsequent flow separation is delayed and its extent is reduced.

Finally, Fig. 6 shows the variation of the velocity profile at the diffuser end for the reference straight wall diffuser compared with the best optimum diffuser. The velocity profiles at the diffuser exit are normalized based on the average inlet velocity. With respect to Fig. 6, the velocity profile in the reference straight wall diffuser shows a recirculation zone at the top wall. This also corroborates the streamline pattern shown in Fig. 4.

(a)

Fig. 6. Velocity Profiles at the diffuser exit.

(b)

In this section the details of optimization process for the plane symmetric diffuser at Re=100 and the fixed diffuser length of L=3H for the case of five control points are examined. As mentioned earlier, for this optimization problem with seven design variables, 70 initial sample points are generated by Space-Filling Latin Hypercube Sampling (SFLHS) method. Under the condition of $\varepsilon=1\times10^{-6}$, 88 iterations are needed to obtain the optimum solution. As reported by (Ghosh *et al.* 2009) in a similar optimization problem using GA with population size of 40 at least 16 generations or 640 exact evaluations were necessary. Here, the number of total iterations including initial sampling and exact evaluations is one fourth of evolutionary (GA) optimization exact evaluations. So, in comparison with evolutionary optimization methods (e.g. GA) coupling Navier-Stokes Computational Fluid Dynamic with expected improvement approach maximization and surrogate modeling can reduce computational runs significantly.

The maximum C_P obtained from computations is 0.476. In order to examine other near optimal points obtained by this methodology the optimal points with the range of $C_P \geq 0.475$ are summarized in Table 4.

(c)

5. CONCLUSIONS

In the present work a passive control of boundary layer separation in a two-dimensional symmetrical diffuser by constrained shape optimization of the diffuser wall has been investigated. The final goal is to increase the pressure recovery inside the diffuser by delaying the flow separation and reducing its extent.

The adopted fully automated methodology of optimization based on geometry parameterization by NURBS, mesh generation by Gambit, CFD simulation by Fluent and Kriging surrogate modeling has been developed on the Matlab platform.

Reasonably high efficiency and performance are confirmed by comparing the optimization results with those of the straight wall diffuser design.
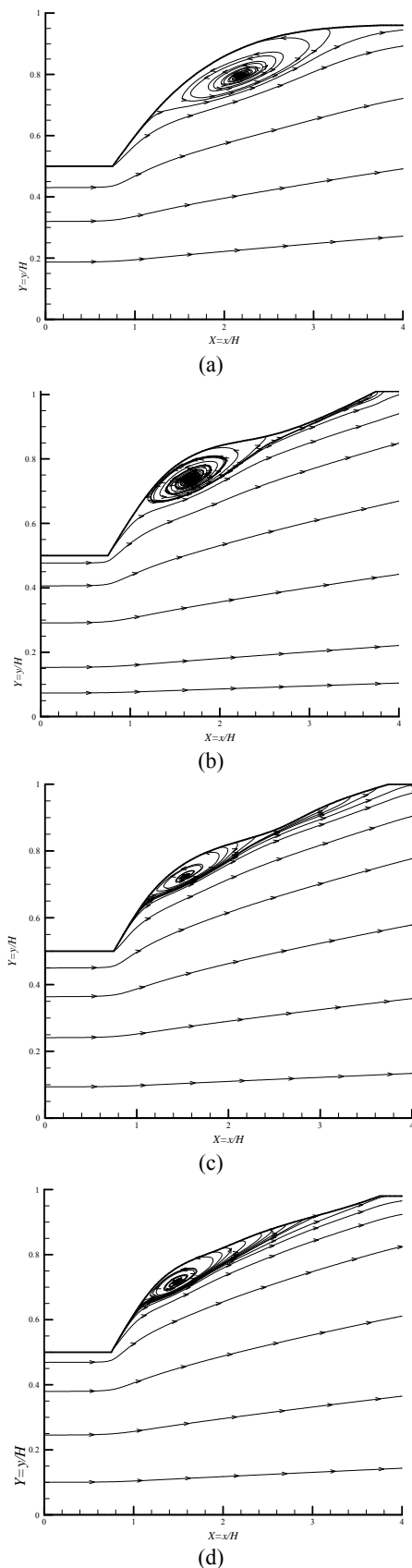

(d)

Fig. 5. the optimum half shape of the diffuser and the corresponding streamline pattern for all control points: (a) three control point; (b) four control points; (c) five control points; (d) six control points.
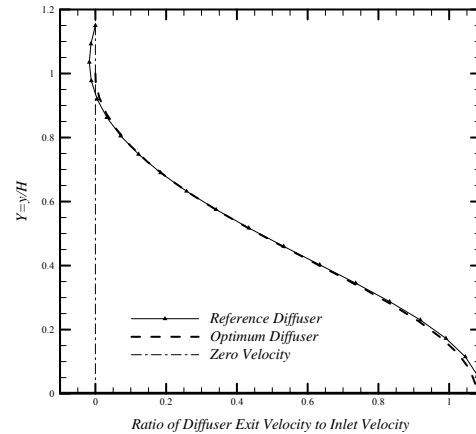
Table 3 The predicted separation and reattachment positions for various design options

Diffuser	1st Separation	1st Reattachment	2nd Separation	2nd Reattachment
Ref	2.25H	5.65H	-------	-------
n_{cp}=3, n_{dv}=3	1.288H	3.33H	-------	-------
n_{cp}=4, n_{dv}=5	1.136H	2.57H	3.598H	3.82H
n_{cp}=5, n_{dv}=7	1.136H	2.267H	2.95H	3.52H
n_{cp}=6, n_{dv}=9	1.135H	2.72H	-------	-------

Table 4 Values of C_P in the optimal region and their positions for the case of five control points

Iteration	C_P	No.	X cord	Y cord	AR
15	0.47501	1st 2nd 3rd 4th 5th	0.75H 1.08H 2.65H 2.86H 3.75H	0.5H 0.66H 0.87H 0.92H 0.96H	1.92
48	0.47573	1st 2nd 3rd 4th 5th	0.75H 1.19H 2.54H 3.06H 3.75H	0.5H 0.68H 0.87H 0.94H 1.03H	2.06
67	0.47564	1st 2nd 3rd 4th 5th	0.75H 1.08H 2.61H 2.85H 3.75H	0.5H 0.64H 0.88H 0.93H 1.03H	2.06
71	0.47503	1st 2nd 3rd 4th 5th	0.75H 1.28H 2.51H 3.02H 3.75H	0.5H 0.73H 0.86H 0.94H 1.03H	2.06

Based on the study, the best diffuser design flow separates at the initial part of diffuser but reattaches immediately downstream, forming a recirculation region; furthermore, the subsequent flow separation is delayed and its extent is reduced. Also, the proposed fully automated constrained shape optimization methodology shows its validity for symmetric diffuser design. Finally, the results show that the total numbers of exact solutions are approximately one fourth of similar evolutionary optimization procedure based on genetic algorithm and reduce computational time and effort significantly.

REFERENCES

Booker, A. J., J. E. Dennis, P. D. Frank, D. B. Serafini, V. Torczon and M. Trosset (1999). A rigorous framework for optimization of expensive functions by surrogates. *Structural Optimization 17(1), 1–13.*

Çabuk, H. and V. Modi (1992). Optimum Plane Diffusers in Laminar Flow. *Journal of Fluid Mechanics 237, 373-393.*

Cholaseuk, D., V. Srinivasan and V. Modi (1999). Shape Optimization for Fluid Flow Problems Using Bezier Curves and Designed Numerical Experiments. *Proceedings of the ASME Design Engineering Technical Conferences, Las Vegas, Nevada, September.*

Fan, H. Y., G. S. Dulikravich and Z. X. Han (2005). Aerodynamics data modeling using support machines. *Inverse Problem in Science and Engineering 13(3), 261–278.*

Forrester, A., A. Sóbester and A. Keane (2008). *Engineering design via surrogate modelling: A practical guide*, John Wiley and Sons, United Kingdom.

Ghosh S., D. K. Pratihar, B. Maiti and P. K. Das (2010). An evolutionary optimization of diffuser shapes based on CFD simulations. *International Journal For Numerical Methods In Fluids 63, 1147-1166.*

Huang, D., T. T. Allen, W. I. Notz and R. A. Miller

(2006). Sequential Kriging optimization using multiple-fidelity evaluations. *Structural Multidisciplinary Optimization 32(5), 369–382.*

HyoGil, B., S. Park and J. Kwon (2013). Efficient global optimization for S-duct diffuser shape design. *Journal of Aerospace Engineering 227(9), 1516–1532.*

Jin, Y. A. (2005). Comprehensive survey of fitness approximation in evolutionary computation. *Soft Computing 9(1), 3–12.*

Johnson, M. E., L. M. Moore and D. Ylvisakar (1990). Minimax and maximin distance designs. *Journal of Statistical Planning and Inference 26, 131–148.*

Jones, D. R. (2001). A taxonomy of global optimization methods based on response surfaces. *Journal of Global Optimization 21, 345–383.*

Keane, A. J. and P. B. Nair (2005). *Computational approaches for aerospace design: The pursuit of excellence*, John Wiley and Sons, United Kingdom.

Madsen, J. I., W. R. Shyy and T. Haftka (2000). Response surface techniques for diffuser shape optimization. *AIAA Journal 38(7), 1512–1518.*

Mariotti, A., A. N. Grozescu, G. Buresti and M. V. Salvetti (2013). Separation control and efficiency improvement in a 2D diffuser by means of contoured cavities. *European Journal of Mechanics B/Fluids 41, 138-149.*

Marjavaara, B. D., T. S. Lundstrom, T. Geol, Y. Mack and W. Shyy (2007). Hydraulic turbine diffuser shape optimization by multiple surrogate model approximations of Pareto fronts. *Journal of Fluids Engineering 129(9), 1228-1240.*

Morris, M. D., and T. J. Mitchell (1995). Bayesian design and analysis of computer experiments: Two examples. *Journal of Statistical Planning and Inference 43, 381-402.*

Queipo, N. V., R. T. Haftka, W. Shyy, T. Goel, R. Vaidyanathan and P. K. Tucker (2005). Surrogate based analysis and optimization. *Progress in Aerospace Sciences 41(1), 1-28.*

Simpson, T. W., J. D. Peplinsk, P. N. Koch and J. K. Allen (2001). Metamodels for computer-based engineering design: survey and recommendations. *Engineering with Computers 17(2), 129-150.*

Svenningsen, K. H., J. I. Madsen, N. H. Hassing and W. H. G. Päuker (1996). Optimization of Flow Geometries Applying Quasi-Analytical Sensitivity Analysis. *Applied Mathematical Modeling 20, 214-224.*